THE JOURNAL OF COMPARATIVE NEUROLOGY 511:678–691 (2008)

Acetylcholine Innervation of the Adult Rat Thalamus: Distribution and Ultrastructural Features in Dorsolateral Geniculate, Parafascicular, and Reticular Thalamic Nuclei

MARTIN PARENT[1] AND LAURENT DESCARRIES[1–3]*
Departments of [1]Pathology & Cell Biology and of [2]Physiology, and [3]Groupe de recherche sur le système nerveux central (GRSNC), Faculty of Medicine, Université de Montréal, Montreal, Quebec, Canada H3C 3J7

ABSTRACT

The acetylcholine (ACh) innervation of thalamus arises mainly from the brainstem pedunculopontine and laterodorsal tegmental nuclei. By using immunocytochemistry with a monoclonal antibody against whole rat choline acetyltransferase (ChAT), we quantified the distribution and characterized the ultrastructural features of these nerve terminals (axon varicosities) in the dorsolateral geniculate (DLG), parafascicular (PF), and reticular thalamic (Rt) nuclei of adult rat. The regional density of ACh innervation was the highest in PF (2.1×10^6 varicosities/mm^3), followed by Rt (1.7×10^6) and DLG (1.3×10^6). In single thin sections, ChAT-immunostained varicosity profiles appeared comparable in shape and content in the three nuclei, but significantly larger in PF than in DLG and Rt. The number of these profiles displaying a synaptic junction was also much higher in PF than in DLG and Rt, indicating that all ChAT-immunostained varicosities in PF were synaptic, but only 39% in DLG and 33% in Rt. The hypothesis that glutamate corelease might account for the maintenance of the entirely synaptic ACh innervation in PF was refuted by the lack of colocalization of ChAT and vesicular glutamate transporter 2 (VGLUT2) in PF axon varicosities after dual immunolabeling. These data suggest that diffuse as well as synaptic transmission convey modulatory effects of the ACh input from brainstem to DLG and Rt during waking. In contrast, the entirely synaptic ACh input to PF should allow for a direct relaying of the information from brainstem, affecting basal ganglia function as well as perceptual awareness, including attention and pain perception. J. Comp. Neurol. 511:678–691, 2008.

Indexing terms: cholinergic innervation; regional distribution; ultrastructure; ChAT immunocytochemistry; stereology; electron microscopy

In the central nervous system (CNS), acetylcholine (ACh) is implicated in the control of a wide variety of neural states and functions, such as plasticity of sensory maps, attention, learning, and memory (Hasselmo, 1995; Dykes, 1997; Baxter and Chiba, 1999; Sarter et al., 2003, 2005). Maximally released in cerebral cortex and thalamus during waking and paradoxal sleep (Steriade and McCarley, 2005), ACh has long been known to play an important role in the regulation of the sleep/waking cycle (Richter and Crossland, 1949; Jasper and Tessier, 1971;

Additional Supporting Information may be found in the online version of this article.

Grant sponsor: Canadian Institutes of Health Research; Grant number: NRF-3544 (to L.D.); Grant sponsor: Fonds de la recherche en santé du Québec (infrastructure grant: GRSNC, and postdoctoral fellowship to M.P.); Grant sponsor: Herbert H. Jasper fellowship from the GRSNC (to M.P.).

*Correspondence to: Laurent Descarries, MD, Department of Pathology and Cell Biology, Université de Montréal, Pavillon Roger-Gaudry, 2900 Boul. Édouard-Montpetit, Montreal, Quebec, Canada H3C 3J7.
E-mail: laurent.descarries@umontreal.ca

Received 5 June 2008; Revised 23 July 2008; Accepted 31 August 2008
DOI 10.1002/cne.21868
Published online in Wiley InterScience (www.interscience.wiley.com).

Jiménez-Capdeville and Dykes, 1996). Because of the strong involvement of the thalamus in the control of states of vigilance, there is a wealth of information on the electrophysiological effects of ACh in this brain region (Steriade and McCarley, 2005). Whereas in specific relay nuclei, such as the dorsolateral geniculate nucleus (DLG), and in intralaminar nuclei, such as the parafascicular nucleus (PF), ACh may depolarize thalamocortical neurons directly, it hyperpolarizes the inhibitory neurons in the reticular thalamic nucleus (Rt), with a consequent disinhibition of the thalamocortical cells that brings them closer to their firing threshold (McCormick and Prince, 1986; Steriade, 2004). Thus, through direct depolarization and indirect disinhibition, ACh modifies the state of membrane polarization of thalamocortical neurons, favoring the relaying of inputs from various motor and sensory modalities (Sillito and Kemp, 1983; Donoghue and Carroll, 1987; McKenna et al., 1988; Rasmusson and Dykes, 1988; Steriade et al., 1991).

The ACh innervation of the thalamus arises essentially from the pedunculopontine (PPN) and the laterodorsal (LTD) tegmental nuclei of the brainstem (Mesulam et al., 1983; Sofroniew et al., 1985; Woolf and Butcher, 1986; Hallanger et al., 1987), containing the ACh groups Ch5 and Ch6, respectively, in the nomenclature of Mesulam et al. (1983). For the rat, a minor contribution of the magnocellular neurons in the nucleus basalis of Meynert to the ACh innervation of Rt has also been described (Woolf and Butcher, 1986; Hallanger et al., 1987; Levey et al., 1987; Jourdain et al., 1989). The ACh neurons in brainstem presumably give rise to highly collateralized axons, which pervade many thalamic nuclei (Woolf and Butcher, 1986; Paré et al., 1988; Steriade et al., 1988; Bolton et al., 1993; Spreafico et al., 1993).

Within the thalamus, the distribution of the ACh innervation is highly heterogeneous, as initially described with acetylcholinesterase histochemistry in the rat (Koelle, 1954; Shute and Lewis, 1963, 1967; Jacobowitz and Palkovits, 1974; Parent and Butcher, 1976; Hoover and Jacobowitz, 1979; Albanese and Butcher, 1980; Woolf and Butcher, 1986), cat (Graybiel and Berson, 1980), and monkey (Olivier et al., 1970). Since the early 1980s, immunohistochemical studies carried out with antibodies against the more specific biosynthetic enzyme choline acetyl transferase (ChAT) have substantiated important differences in the density of ACh innervation among thalamic nuclei in the rat (Mesulam et al., 1983; Sofroniew et al., 1985; Ichikawa and Hirata, 1986; Woolf and Butcher, 1986; Levey et al., 1987; Houser et al., 1988), cat (Stichel and Singer, 1985; Vincent and Reiner, 1987; Hoshino et al., 2000), and human (Heckers et al., 1992). However, because of technical limitations, none of these reports could provide unbiased quantitative estimates of the densities of ACh innervation in actual number of axon terminals (varicosities) per volumetric unit of tissue.

With the advent of ChAT immunocytochemistry, there were also many reports on the ultrastructural features of ACh innervation in thalamic nuclei of different species (Isaacson and Tanaka, 1988; Raczkowski and Fitzpatrick, 1989; Hallanger et al., 1990; Houser, 1990; Kuroda and Price, 1991a,b; Beaulieu and Cynader, 1992; Schwartz and Mrzljak, 1993; Patel and Bickford, 1997; Patel et al., 1999), including rat DLG (de Lima et al., 1985; Hallanger et al., 1990) and Rt (Hallanger and Wainer, 1988). Here again, however, despite increasing evidence that, in many parts of the rat CNS, most ACh terminals do not form the junctional membrane specializations that are the hallmark of synapses (for review see Descarries and Mechawar, 2000), a systematic evaluation of the synaptic incidence of thalamic ACh axon varicosities remained to be carried out, leaving open the issue of diffuse vs. synaptic transmission by ACh in this part of the brain.

Several neurochemical investigations have raised the possibility of a corelease of amino acid transmitters or neuropeptides by PPN and LTD neurons, which could support complex forms of signaling in the thalamus (Vincent et al., 1986; Vincent and Kimura, 1992; Lavoie and Parent, 1994). Recent in situ hybridization studies have demonstrated an abundance of mRNA coding for the vesicular glutamate transporter 2 (VGLUT2) in rat brainstem (Herzog et al., 2001), although the precise anatomical localization of VGLUT2 mRNA remains to be determined in this brain region. Low levels of VGLUT1 mRNA have been detected in the inferior olive, the intermediate reticular zone, and the gigantocellular reticular nucleus of the rat brainstem, but not in PPN or LTD (Ni et al., 1994, 1995). VGLUT3 mRNA has been shown to be present in a subpopulation of ACh neurons of the nucleus basalis (Harkany et al., 2003; Nickerson Poulin et al., 2006) and in ACh interneurons of the neostriatum (Fremeau et al., 2002; Gras et al., 2002; Schafer et al., 2002; Herzog et al., 2004), but not in PPN (Herzog et al., 2004). In immunocytochemical studies, both VGLUT1 and VGLUT2 proteins have been demonstrated to be present in thalamic nuclei, including DLG, PF, and Rt (Kaneko et al., 2002), but not VGLUT3 (Kaneko et al., 2002; Varoqui et al., 2002; Herzog et al., 2004; Nickerson Poulin et al., 2006; Graziano et al., 2008). Because VGLUT1 and VGLUT2 mRNA are strongly expressed in the cerebral cortex and the hindbrain, respectively (Hisano, 2003; Fremeau et al., 2004), it is assumed that, in the thalamus, VGLUT1 protein is located solely in corticothalamic axon varicosities and VGLUT2 in axon varicosities originating from the brainstem and spinal cord (Graziano et al., 2008).

It has not yet been determined whether VGLUT3 protein is present in the low proportion of cortical or striatal ACh axon varicosities that make morphologically identifiable synapses (Umbriaco et al., 1994; Contant et al., 1996). However, in the case of dopamine neurons of the mesencephalic tegmentum, the suggestion has already been made that the corelease of glutamate might play a role in the establishment of synaptic junctions by these axon varicosities (Trudeau, 2004; Descarries et al., 2007). For this reason, the present study included double-immunolabeling experiments with ChAT and VGLUT2 antibodies to examine the possibility of a colocalization of this glutamate transporter in synaptic ACh terminals within thalamic nuclei.

Our study focused on DLG, as representative of a specific relay nucleus that contains inhibitory (GABAergic) interneurons in addition to excitatory (glutamatergic) thalamocortical neurons (Ohara et al., 1983; Ottersen and Storm-Mathisen, 1984); PF, as a prominent member of the intralaminar nuclear group entirely composed of glutamatergic neurons that project mainly to the cerebral cortex and neostriatum (Jones and Leavitt, 1974; Nauta et al., 1974; Deschênes et al., 1996; Van der Werf et al., 2002); and Rt, as entirely composed of GABAergic projection neurons sending their axon to other thalamic nuclei (Scheibel and Scheibel, 1966; Houser et al., 1980; Ottersen

and Storm-Mathisen, 1984; de Biasi et al., 1986; Jones, 2007). Some of the results have already been reported in abstract form (Parent and Descarries, 2006, 2007).

MATERIALS AND METHODS

Animals

Twelve adult male Sprague-Dawley rats (Charles River, St. Constant, Quebec, Canada), weighing 275–325 g, were used. All procedures involving animals and their care were conducted in strict accordance with the *Guide to the care and use of experimental animals* (2nd ed) of the Canadian Council on Animal Care. The experimental protocols were approved by the Comité de Déontologie pour l'Expérimentation sur des Animaux at the Université de Montréal.

Primary antibodies

The mouse monoclonal antibody against whole, purified rat brain ChAT protein (ChAT-17) was a generous gift from Boyd K. Hartman and Costantino Cozzari (Cozzari et al., 1990). This antibody displays a high affinity for ChAT (3×10^{11} liter/M), with a specific epitope on the ChAT molecule. Immunoperoxidase labeling of rat or mouse brain sections with this antibody allows for a light and electron microscopic visualization of neuronal cell bodies and their dendritic and axonal arborizations in the distribution and density expected from ACh neurons only (Umbriaco et al., 1994; Contant et al., 1996; Aznavour et al., 2005). Accordingly, after ibotenic acid lesions of the nucleus basalis, there is almost total disappearance of the ChAT immunoreactivity in cerebral cortex, except for interneurons (Cossette et al., 1993), and similar observations have been made after 192 IgG-saporin lesions in the substantia innominata-nucleus basalis regions (Nickerson Poulin et al., 2006). As also reported by these authors, dual immunofluorescence with this antibody and the goat antivesicular ACh transporter AB1578 (Chemicon, Temecula, CA) demonstrates a complete overlap in the cell body labeling of basal forebrain ACh neurons as well as a distribution of ChAT-immunoreactive axons and varicosities in the cerebral cortex highly similar to that reported previously (Umbriaco et al., 1994; Mechawar et al., 2000).

The rabbit polyclonal antibody against a fusion protein containing glutathione S-transferase (GST) and the amino acid 510–582 of the rat vesicular glutamate transporter VGLUT2 was obtained from Synaptic Systems Gmbh (Göettingen, Germany). It has been fully characterized and its specificity verified in previous studies (Takamori et al., 2001; Montana et al., 2004; Anlauf and Derouiche, 2005; Zhou et al., 2007). On Western blot, this VGLUT2 antibody labels a single band at 65 kDa (Takamori et al., 2001; Zhou et al., 2007), corresponding to the molecular weight of VGLUT2. There is no immunolabeling after preincubation of this VGLUT2 antibody with the fusion protein rat VGLUT2/DNPI Strep-Tag (AA 510–582; Zhou et al., 2007).

The rabbit polyclonal antibody against VGLUT3 (P45-3) was a generous gift from Salah El Mestikawy. This antibody was raised against the peptide CETELNHEAFVS-PRKKM (Glu531-Met547) at the C-terminus of VGLUT3 and affinity purified. It detected an intracellular and punctiform signal on BON cells permanently transfected with pcDNA3-VGLUT3 but not with plasmids coding for VGLUT1 or VGLUT2 (Gras et al., 2002). On Western blots of protein extracted from rat brain homogenates, it showed a band at 50–60 kDa, which corresponds to the predicted molecular weight of VGLUT3 (Gras et al., 2005). The immunocytochemical localizations observed in rat brain with this P45-3 antibody were found to be very similar to those obtained with a second anti-VGLUT3 antibody (P45-1) raised in rabbit against a peptide (Asp27-Asp44) at the N-terminus of VGLUT3 (Gras et al., 2002), or with a third anti-VGLUT3 antibody raised in guinea pig against the entire C-terminus (amino acids 522–588) of rat VGLUT3 (Somogyi et al., 2004). There was no immunolabeling in brain with a preimmune serum for P45-3 or with a P45-3 solution saturated with its cognate peptide (Gras et al., 2002).

Immunocytochemistry

Brain tissue intended for light (five rats) and confocal (one rat) microscopy was prepared as follows. After deep anesthesia with sodium pentobarbital (65 mg/kg, i.p.), these rats were perfused transcardially with 50 ml of ice-cold sodium phosphate-buffered saline (PBS; 50 mM; pH 7.4), followed by 500 ml of a fresh solution of 4% paraformaldehyde (PFA) in 0.1 M sodium phosphate buffer (PB; pH 7.4). The brain was rapidly dissected out and postfixed by immersion in the same solution for 24 hours at 4°C. After several washes in PBS, serial transverse 35-μm-thick sections were cut with a vibratome and collected serially in PBS. One of every three sections from five rats was processed for ChAT immunohistochemistry as described below. To help in identifying thalamic nuclei, the second set of adjacent sections was stained for cytochrome oxidase, according to a previously described histochemical protocol (Wong-Riley, 1979), and the third with cresyl violet. Sections from another rat were processed for double immunofluorescence and confocal microscopy as described below.

For electron microscopy, the brains of six rats were fixed by sequential aortic arch perfusion of 50 ml of cold PBS, 150 ml of 4% PFA solution, 250 ml of 4% PFA + 0.1% glutaraldehyde, and 250 ml of 4% PFA. After overnight postfixation by immersion in the 4% PFA solution at 4°C, 50-μm-thick transverse sections were cut with the vibratome, to be processed for ChAT immunocytochemistry and examined in the electron microscope as described below.

Single ChAT immunostaining for light microscopy. The 35-μm-thick sections intended for light microscopy were sequentially incubated, at room temperature, in 1) a blocking solution of PBS containing 5% normal goat serum, 0.5% gelatin, and 0.2% Triton X-100 (2 hours); 2) the same blocking solution to which 2 μg/ml of the mouse monoclonal antibody against ChAT was added (overnight); and 3) the biotinylated goat anti-mouse antibody (Jackson Immunoresearch, West Grove, PA) diluted 1:1,000 in blocking solution (1 hour). After rinses in PBS, sections were incubated for 1 hour in a 1:1,000 dilution of horseradish peroxidase-conjugated streptavidin (Jackson Immunoresearch, West Grove, PA), washed in PBS followed by Tris saline buffer (TBS; pH 7.4), and then immersed for 3 minutes in a cold solution of 0.05% 3,3′-diaminobenzidine (DAB; Sigma, St. Louis, MO) in TBS, to which 0.005% H_2O_2 was added. The reaction was stopped by several washes in TBS followed by PB, and the sections were mounted on gelatin-coated slides, air dried, dehy-

drated in graded alcohol, cleared in toluene, and coverslipped with DPX (Fluka, Sigma-Aldrich, Oakville, Ontario, Canada), to be examined as described below.

Double ChAT/VGLUT immunofluorescence for confocal microscopy. These sections were incubated for 36 hours at room temperature with both mouse anti-ChAT diluted at 2 μg/ml and rabbit anti-VGLUT2 or VGLUT3 primary antibodies, diluted 1:500. After several washes in PBS, they were incubated for 4 hours at room temperature with a mix of Alexa Fluor 568-conjugated goat anti-mouse and Alexa Fluor 488-conjugated goat anti-rabbit IgGs (1:500; Molecular Probes, Eugene, OR), washed in PB and distilled water, and mounted on microscope slides in Vectashield mounting medium for fluorescence (Vector Laboratories, Burlingame, CA). Controls for these double-labeling experiments included omission of one of the primary antibodies. There was no cross-reactivity of the secondary antibodies. Images were captured with a confocal microscope (Leica TCS-SP1) using sequential laser analysis and processed in Adobe Photoshop (v. CS2; Adobe Systems, San Jose, CA).

Single ChAT immunostaining for electron microscopy. Fifty-micrometer-thick sections from four rats were prepared as described above for light microcopy, but without Triton X-100 in all solutions. After revelation in DAB, these sections were osmicated, dehydrated in ethanol and propylene oxide, and flat embedded in Durcapan (Fluka), as previously described in detail (Riad et al., 2000). Rectangular pieces within DLG, PF, and Rt were removed from the flat-embedded ChAT-immunostained sections, glued to the tip of resin blocks, and sectioned ultrathin (80 nm) with a Reichert Jung ultramicrotome. These sections were collected on bare 150-mesh copper grids, stained with lead citrate, and examined with a Phillips CM100 electron microscope (60 kV; Philips Electronique, St. Laurent, Quebec, Canada). In these experiments, immunocytochemical controls included omission of the primary or the secondary antibody, which completely abolished the immunostaining. This material was examined as described below.

Double ChAT/VGLUT2 immunolabeling for electron microscopy. Sections from two rats were incubated for 60 hours at 4°C with both the mouse anti-ChAT and the rabbit anti-VGLUT2 primary antibodies, diluted 2 μg/ml and 1:500, respectively. The immunoperoxidase reaction was then performed as described above, with DAB as the chromogen to reveal ChAT, and the sections were incubated for 24 hours at room temperature in goat anti-rabbit IgG conjugated to 1-nm colloidal gold particles (AuroProbe One; Amersham, Oakville, Ontario, Canada) diluted 1:50 to reveal VGLUT2. The sections were then treated with an IntenSE kit (Amersham) to increase the size of immunogold particles and processed for electron microscopy as described above. Controls included omission of either one of the primary antibodies to exclude cross-reactivity of the secondary antibodies.

Quantitative assessment of the density of ChAT-immunostained innervation in DLG, PF, and Rt

An unbiased stereological approach was used to estimate the number of ChAT-immunostained axon varicosities in DLG, PF, and Rt (see Fig. 1). A light microscope (Leica DM 6000B) equipped with a digital camera (Optronics microfire), a motorized stage (X and Y axes), and a Z-axis indicator (Leica Z axis control) was used. This system was controlled by a computer running StereoInvestigator software (v. 7.00.3; MicroBrightField, Colchester, VT).

Five equally spaced transverse sections across the entire volume of each nucleus were selected. Intervals between sections corresponded to 315 μm in DLG, 105 μm in PF, and 420 μm in Rt. At low magnification, the contours of nuclei were traced in the left thalamus, with the help of adjacent cytochrome oxidase sections as a guide. The sampling process leading to estimations of the total number of ACh axon varicosities in each thalamic nucleus began by randomly translating a grid formed by 138 × 126 μm squares over the section. At each intersection of the grid that fell into the nucleus, a counting frame measuring 25 × 25 μm was drawn and examined with a ×100/1.30 oil objective. In the light microscope, ChAT-immunostained varicosities appear as round or ovoid dilations of ChAT-labeled axons (see Fig. 2). Varicosities that fell within the counting frame and that did not contact the exclusion lines were counted whenever they came into focus within a 12-μm-thick optical dissector positioned 1 μm below the surface of the tissue. The thickness of the mounted tissue was measured at regular intervals during the process, yielding mean values between 14.1 and 16.8 μm for the ChAT-stained sections. For each thalamic nucleus, the density of ACh innervation was then expressed in millions of varicosities per cubic micrometer of tissue, using the total number calculated by the optical dissector and the volume of the nucleus estimated in ChAT-immunostained sections by Cavalieri's method.

A similar unbiased stereological approach was used on adjacent Nissl-stained sections to estimate the total number of neurons in each of the three thalamic nuclei, delineated, as above, with the help of adjacent cytochrome oxidase-stained sections. Sampling sites were randomly positioned at the intersection of a grid formed by 350 × 350 μm squares. The volume of the optical dissector was 100 × 100 × 14 μm. Counting was performed with a ×40/0.85 objective. Neurons stained with cresyl violet display a faintly stained cytoplasm but a dark nucleus and sharp nucleolus. Only neurons with a nucleolus in focus within the optical dissector were counted. The mean thickness of the cresyl violet-stained sections ranged between 16.3 and 19.1 μm. The number of axon varicosities in each nucleus was then divided by the number of neurons provided by the counting system, to estimate the average number of ChAT-immunoreactive axon varicosities per neuron.

On average, 9,563 axon varicosities and 864 neurons were counted in each rat. Average of the Gunderson ($m = 1$) and the second estimated coefficient of error (Schmitz-Hof) yielded values ranging between 0.02 and 0.05 for axon varicosities and cell bodies counted in the three thalamic nuclei.

Electron microscopic examination of the ChAT-immunostained axon varicosities

After single (ChAT) or dual (ChAT and VGLUT2) immunolabeling, ChAT-immunostained axon varicosities were readily identified in the electron microscope as round or ovoid axon dilations, more than 0.25 μm in transverse diameter, containing aggregated synaptic vesicles and often a mitochondrion. These profiles were filled by a fine

DAB immunoprecipitate of variable density, which often lined the plasma membrane and the outer surface of organelles. After single labeling for ChAT, immunostained varicosities were sampled at a working magnification of ×15,500, by taking a picture of every such profile encountered, until more than 100 were obtained from each nucleus in each rat. These pictures were printed at a final magnification of ×39,000, and the first 50 or so ChAT-immunostained varicosity profiles with a full contour and distinct content were kept for analysis. Equivalent numbers of unlabeled profiles were selected at random from the same prints. For this purpose, a transparent overlay bearing a fixed mark in its upper left quadrant was used to identify the nearest fully visible unlabeled axon varicosity in each print. The ChAT-immunostained and randomly selected unlabeled varicosities were then measured for cross-sectional area and for short and long axes, using the public-domain Image J software from NIH (v. 1.61). The varicosities were also classified as containing a mitochondrion or not and as showing a synaptic complex or not, i.e., a localized straightening of apposed plasma membranes associated with a slight widening of the intercellular space and a thickening of the pre- and/or postsynaptic membrane. The synaptic junctions were further characterized as symmetrical or asymmetrical, the synaptic targets were identified, and the length of junctional complexes was measured.

The synaptic incidence observed in single sections could then be extrapolated to the whole volume of varicosities by means of a stereological formula (Beaudet and Sotelo, 1981), using the long axis as diameter (Umbriaco et al., 1994). This formula considers the varicosities as spheres and takes into account the average size of varicosity profiles, the length of their junctional complexes, and the thickness of the section, to predict the probability of seeing a synapse if there is one made by each varicosity. The synaptic incidence is then inferred by comparison with this predicted value. In the study of Umbriaco et al. (1994), the reliability of this extrapolation was verified experimentally by examining a large population of ChAT-immunostained cortical varicosities both in serial sections across their entire volume and as a randomized, single-section sample.

Statistical analysis

One-way ANOVA and Tukey's multiple-comparisons tests were used to detect significant differences in volume, neuronal counts, regional density of ACh innervation, number of ChAT-immunostained varicosities per neuron, and dimensions and synaptic incidence of ChAT-immunostained or unlabeled varicosity profiles among the three thalamic nuclei. Differences were considered significant at $P < 0.05$.

RESULTS

Density of ChAT-immunostained innervation in DLG, PF, and Rt

A similar regional distribution of ChAT immunostaining was observed in the thalamus of the five rats examined by light microscopy. In accordance with earlier descriptions (Sofroniew et al., 1985; Ichikawa and Hirata, 1986; Levey et al., 1987; Houser et al., 1988), the overall density of ChAT immunostaining varied markedly between the different thalamic nuclei (Fig. 1). The medial habenula showed the strongest immunoreactivity, because of its content in small, round and closely packed, darkly immunostained cell bodies, giving rise to the numerous, relatively large, nonvaricose axons visible in the adjacent fasciculus retroflexus. In all other thalamic nuclei, the immunolabeling was exclusively axonal.

The density of ChAT immunostaining was low in motor thalamic nuclei (ventroanterior, ventrolateral, ventromedial) and moderate in the sensory relay nuclei (DLG, ventroposterior, posterior), except for the medial geniculate nucleus, in which it was rather low. In so-called association nuclei, it was high in the mediodorsal nucleus, moderate in the lateral nuclei (lateral, posterior, laterodorsal), and low in the anterior nuclei (anterodorsal, anteromedial, interanteromedial). As noted previously (Sofroniew et al., 1985), the ventrolateral part of the anteroventral nucleus was more densely ChAT immunoreactive than its dorsomedial part (Fig. 1A). The immunostaining ranged from moderate to strong in the midline (paraventricular, paratenial, intermediodorsal), intralaminar (centralateral, PF), and intermediate (central medial, paracentral) nuclei, with the paraventricular nucleus the less and the central medial nucleus the most densely innervated. Rt was strongly immunoreactive.

As observed by light microscopy, there were no striking differences in the overall configuration of the intricate network of fine, varicose ChAT-immunostained axons that pervaded all parts of DLG, PF, and Rt (Fig. 2). Several thicker, nonvaricose immunostained axons, indicative of fibers en passage, were seen in DLG and Rt, but not in PF. In transverse sections of DLG, some of these relatively thick, nonvaricose fibers could be followed across the entire extent of the nucleus.

As measured with Cavalieri's method, the respective volumes of DLG, PF, and Rt were 0.82 ± 0.06, 0.25 ± 0.02, and 0.76 ± 0.11 mm^3 (PF < DLG and Rt, $P < 0.01$). In cresyl violet-stained sections, the neuronal cell bodies in DLG, PF, and Rt were of comparable size and shape, averaging 15.8 ± 0.7 μm in diameter. As estimated with StereoInvestigator, the neuronal density was the highest in PF ($51{,}465 \pm 3{,}577$ neurons/mm^3), followed by DLG ($40{,}069 \pm 1{,}540$) and Rt ($31{,}884 \pm 3{,}351$; PF > DLG, $P < 0.05$; PF > Rt, $P < 0.01$). The number of ChAT-immunostained varicosities per cubic micrometer of tissue (i.e., the regional density of ChAT innervation) was also the highest in PF (2.1 ± 0.2 million ChAT-immunostained axon varicosities/mm^3), followed by Rt (1.7 ± 0.2 million) and DLG (1.3 ± 0.1 million; Fig. 3). However, Rt was more densely innervated than PF in number of ChAT-immunostained varicosities per neuron. There were 57 ± 7 ChAT-immunostained varicosities per neuron in Rt, 43 ± 5 in PF, and 32 ± 2 in DLG. The ChAT innervation of DLG was the least dense, in terms both of regional density and of number of axon varicosities per neuron (Fig. 3).

Ultrastructural features of ChAT-immunostained axon varicosities in DLG, PF, and Rt

The ChAT-immunostained axon varicosities in DLG, PF, and Rt shared many ultrastructural features (Fig. 4). Arising from thin, unmyelinated axons, they were generally ovoid and contained numerous, more or less tightly

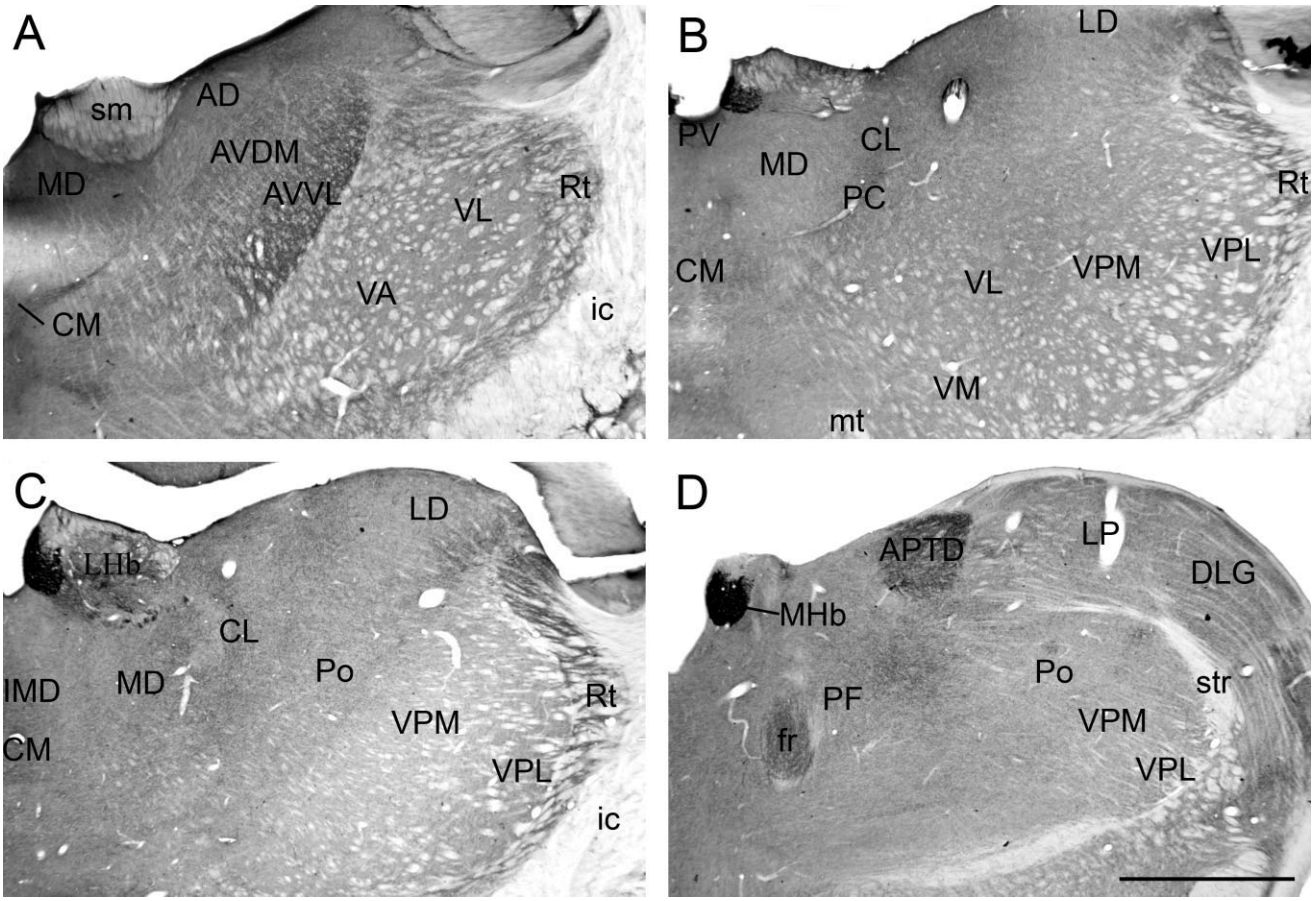

Fig. 1. ChAT-immunostained hemisections at four equally spaced, rostrocaudal, transverse levels across the thalamus (**A–D**), approximately 1.8, –2.6, –3.4, and –4.2 mm behind bregma, respectively (Paxinos and Watson, 2005). Note the heterogeneous distribution of the immunolabeling, which essentially reflects the density of ACh innervation, except in the medial habenula, where ChAT positive perikarya are present. AD, anterodorsal; APTD; anterior pretectal/dorsal; AVDM, anteroventral/dorsomedial; AVVL, anteroventral/ventrolateral; CL, centrolateral; CM, central medial; DLG, dorsolateral geniculate; fr, fasciculus retroflexus; ic, internal capsule; IMD, intermediodorsal; LD, laterodorsal; LHb, lateral habenula; LP, lateral posterior; MD, mediodorsal; MHb, medial habenula; mt, mammillothalamic tract; PC, paracentral; PF, parafascicular; Po, posterior thalamic nuclear group; PV, paraventricular; Rt, reticular; sm, stria medullaris; str, superior thalamic radiation; VA, ventroantrior; VL, ventrolateral; VM, ventromedial; VPL, ventral posterolateral; VPM, ventral posteromedial. Scale bar = 1 mm.

aggregated, small and clear vesicles, often associated with one or more mitochondria. As shown in Table 1, the ChAT-immunostained varicosity profiles were of similar size in DLG and Rt but significantly larger in PF. Their mean diameter ranged from 0.3 to 1.5 μm in DLG, 0.3 to 1.4 μm in Rt, and 0.3 to 2.3 in PF, for respective averages of 0.6, 0.6, and 0.8 μm. The unlabeled axon varicosity profiles in PF were also larger than those in DLG and Rt. The proportion of ChAT profiles showing one or more mitochondria was higher than that of randomly selected, unlabeled varicosities, a difference reaching statistical significance in PF (Table 1).

ChAT-immunostained varicosity profiles displaying or not a synaptic junction were observed in all three thalamic nuclei (Fig. 4). The proportion of ChAT-immunostained varicosity profiles exhibiting a junctional complex in single thin sections was significantly higher in PF (25%) than in DLG (8%) and Rt (10%). Moreover, in DLG and RI, the observed frequency of junctions was markedly lower for the ChAT-immunostained than for the unlabeled varicosity profiles (Table 2). When extrapolated to the whole volume of varicosities with the stereological formula of Beaudet and Sotelo (1981), the synaptic incidence for whole ChAT-immunostained varicosities in PF amounted to 109%, suggesting that this ACh innervation is entirely synaptic. In contrast, in both DLG and Rt, the extrapolation indicated that the ACh innervation is largely asynaptic, with only 33% of the varicosities in DLG and 39% of the varicosities in Rt making a synapse (Table 2). The very high (>100) percentages extrapolated for the unlabeled varicosities in the three nuclei indicated that the vast majority of these axon varicosities were synaptic and that a considerable number made more than one synaptic contact.

Much as the randomly selected unlabeled terminals in the same nuclei, the synaptic ChAT-immunostained varicosities contacted dendritic branches more frequently than spines in PF and Rt, but spines more frequently than branches in DLG (Table 2). This seemed to be associated with a greater frequency of symmetrical vs. asymmetrical

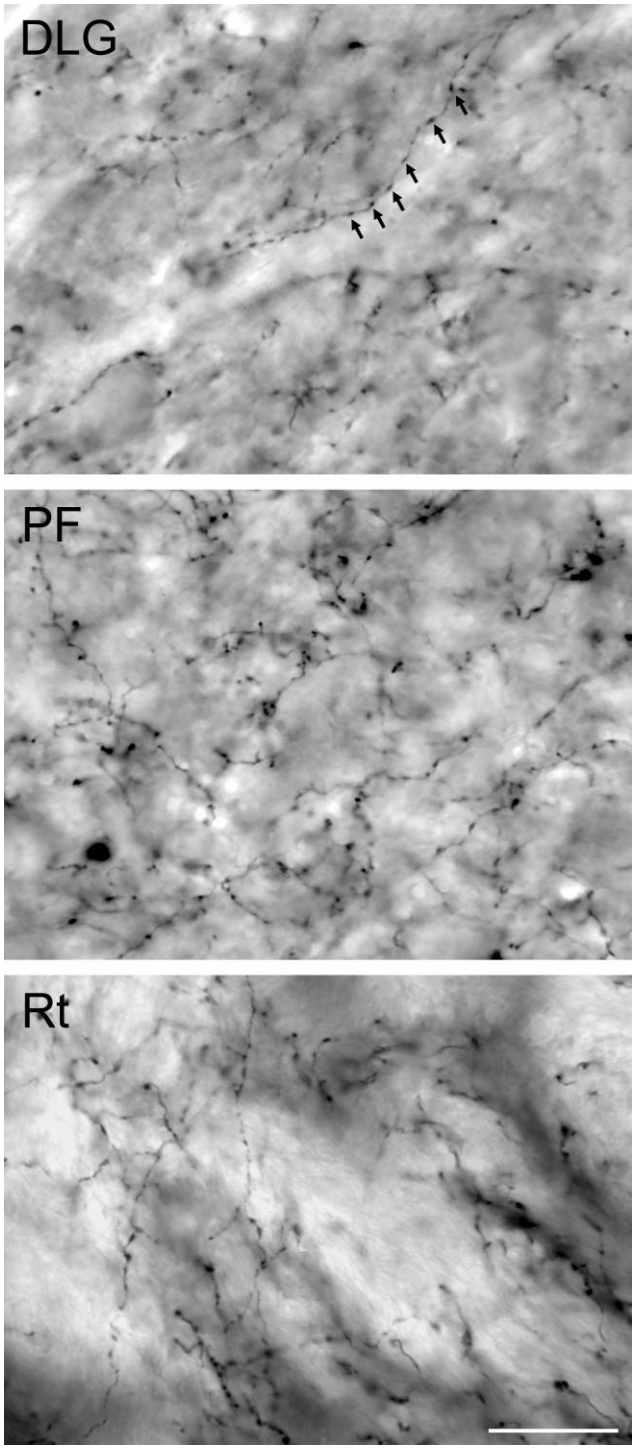

Fig. 2. Photomicrographs at a higher magnification showing the terminal arborization of ChAT-immunostained axons in DLG, PF, and Rt. In all three nuclei, these thin axonal branches display rather equally spaced varicosities, of variable size along the same fiber (e.g., small arrows in DLG). The overall pattern of innervation appears similar in the three thalamic nuclei. No pericellular arrangements are visible. Scale bar = 20 μm.

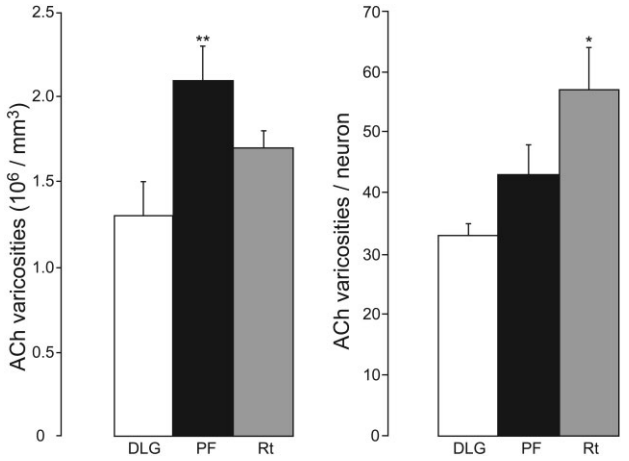

Fig. 3. **Left:** Density of ACh innervation (10^6 ChAT-immunostained varicosities per cubic millimeter of tissue) in DLG (white), PF (black), and Rt (gray), as measured with an unbiased stereological method (for details see Materials and Methods). **Right:** Number of ChAT-immunostained axon varicosities per neuron in the three thalamic nuclei. Means ± SEM from five rats. *$P < 0.05$, **$P < 0.01$ vs. DLG.

contacts made by the ChAT-immunostained as well as unlabeled varicosities in PF and Rt compared with DLG, but the small number of synaptic ChAT-immunostained varicosities in Rt and DLG precluded a statistical validation of this relationship. A rare example of ChAT-immunostained axon varicosity in close apposition to a DLG cell body is shown in Figure 4A. It is noteworthy that, in all three thalamic nuclei, including PF, no axosomatic ACh synapses were observed. ChAT-immunostained varicosities were often seen in direct apposition to, but never making a synaptic junction with, other, unlabeled axon terminals.

Lack of dual ChAT and VGLUT2 immunolabeling

As illustrated in Figure 5A, in the confocal microscope, abundant punctate labeling suggestive of axon varicosities was visualized in PF with either Alexa Fluor 568 (magenta, ChAT) or Alexa Fluor 488 (green, VGLUT2) fluorophore. However, there was not a single instance of an axon varicosity labeled with the two dyes in merged images. In contrast, in tissue processed as a technical control with the same secondary antibodies and fluorophores, many dually labeled axon varicosities with ChAT and VGLUT3 antibodies were present in the neostriatum (see Supporting Information).

In keeping with this result, there were many axon varicosities displaying either ChAT (immunoperoxidase DAB) or VGLUT2 (immunogold) immunolabeling that could be observed in PF after the dual immunolabeling for electron microscopy (Fig. 5B–D), but no axon varicosity displaying both labeling, after examination of more than 80 ChAT- and 120 VGLUT2-positive axon varicosities. As in PF, no dually labeled axon varicosities were observed in DLG and Rt by confocal or electron microscopy (data not shown).

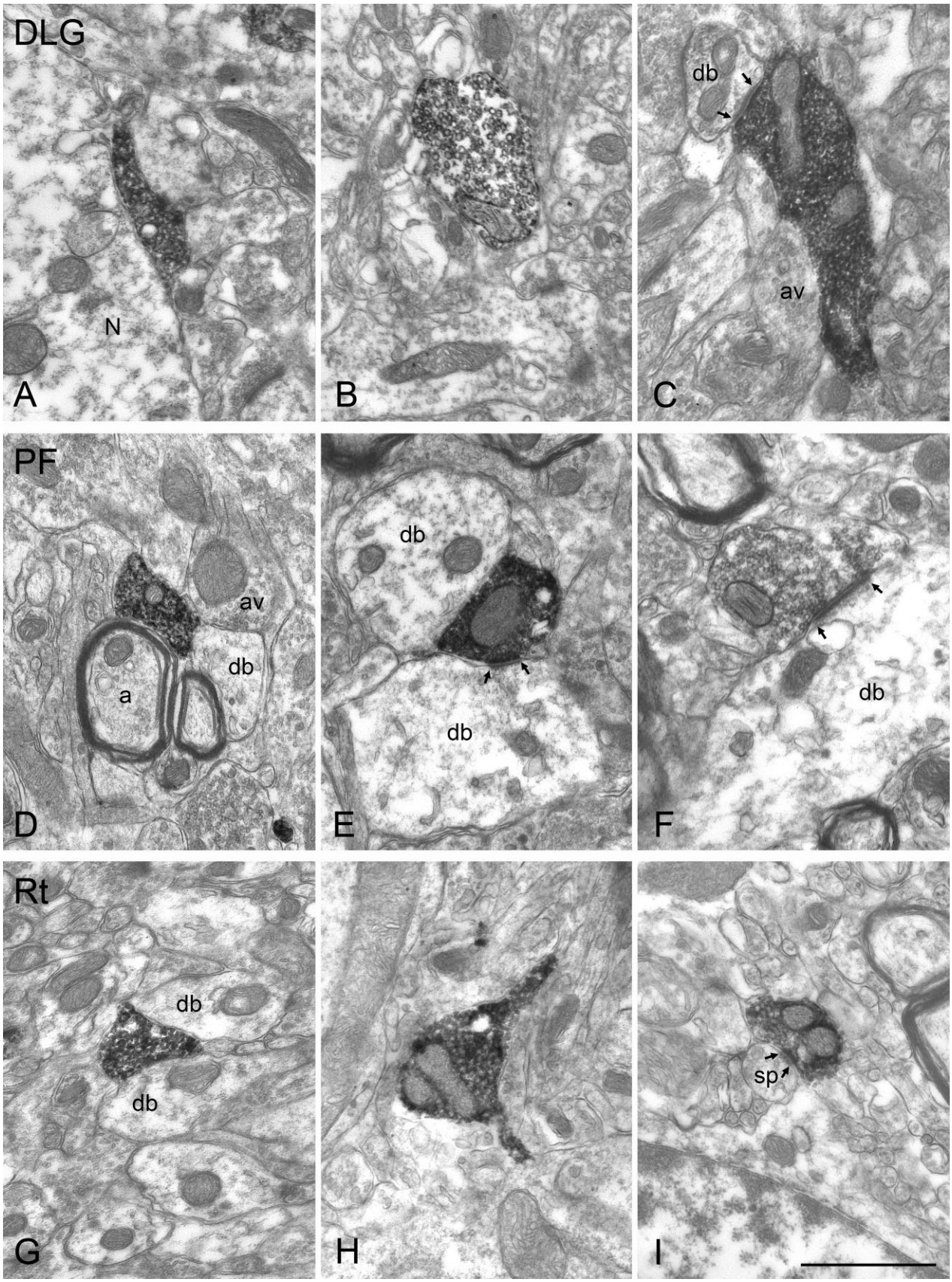

Fig. 4. Examples of ACh axon varicosities in DLG (**A–C**), PF (**D–F**), and Rt (**G–I**) of adult rat thalamus. The ChAT-immunostained axon varicosities appear similar in shape and vesicular content in the three nuclei but, on average, are significantly larger in PF than in DLG and Rt (see Table 1). In A (DLG), the immunostained varicosity is directly apposed to a neuronal cell body (N) but does not display any area of synaptic membrane specialization, nor does that shown in B. That in C is seen to make a synaptic contact (between small arrows) with a dendritic branch (db). Among the three axon varicosities in PF, two (E,F) exhibit a synaptic junction (between small arrows) on a db. In F, the junctional complex is clearly asymmetrical. In Rt (G–I), only the relatively small ACh varicosity profile in I shows a synaptic junction (between small arrows), which is made with a dendritic spine (sp). In H, note the presence of synaptic vesicles in the short segments of unmyelinated axon leading into the varicosity. Scale bar = 1 μm.

TABLE 1. Morphometric Features of ChAT-Immunostained (ACh) Versus Randomly Selected Unlabeled Axon Varicosities

	Dorsolateral Geniculate		Parafascicular		Reticular	
	ACh	Unlabeled	ACh	Unlabeled	ACh	Unlabeled
Number examined	205	205	190	190	173	173
Dimensions						
Short axis (μm)	0.41 ± 0.01	0.47 ± 0.02	0.57 ± 0.07†	0.57 ± 0.03	0.40 ± 0.02	0.47 ± 0.01
Long axis (μm)	0.83 ± 0.03	0.88 ± 0.02	0.99 ± 0.05†	1.01 ± 0.02	0.82 ± 0.03	0.94 ± 0.02
Aspect ratio	2.10 ± 0.06	2.02 ± 0.06	2.00 ± 0.05	1.89 ± 0.12	2.14 ± 0.02	2.21 ± 0.07
Diameter (μm)	0.62 ± 0.01	0.67 ± 0.02	0.78 ± 0.06†	0.79 ± 0.02	0.61 ± 0.02	0.70 ± 0.01
Area (μm^2)	0.30 ± 0.01	0.37 ± 0.02	0.47 ± 0.05††	0.51 ± 0.03	0.29 ± 0.02	0.39 ± 0.01
% with mitochondria	50 ± 5	34 ± 4	65 ± 5*	44 ± 3	57 ± 6	41 ± 3

The unlabeled profiles were selected at random from the same micrographs displaying the ChAT-immunostained profiles, as explained in Material and Methods. Means ± SEM from 4 rats. *$p < 0.05$ for ACh versus unlabeled. †$p < 0.05$ and ††$p < 0.01$ for PF versus DLG and Rt.

TABLE 2. Junctional Features of ChAT-Immunostained (ACh) Versus Randomly Selected Unlabeled Axon Varicosities

	Dorsolateral Geniculate		Parafascicular		Reticular	
	ACh (205)	Unlabeled (205)	ACh (190)	Unlabeled (190)	ACh (173)	Unlabeled (173)
Synaptic incidence (%)						
Single sections	8 ± 1*** (17)	46 ± 3 (95)	25 ± 2*†† (48)	37 ± 3 (70)	10 ± 2*** (17)	45 ± 3 (78)
Whole volume	33 ± 6***	185 ± 14	109 ± 18†	161 ± 17	39 ± 10***	174 ± 10
Length of synaptic junctions (μm)	0.20 ± 0.01	0.22 ± 0.01	0.25 ± 0.03	0.25 ± 0.02	0.19 ± 0.02*	0.26 ± 0.01
Synaptic target (%)						
Dendritic branches	39 ± 3 (6)	41 ± 6 (37)	69 ± 7 (32)	51 ± 5 (35)	65 ± 18 (9)	55 ± 7 (42)
Dendritic spines	61 ± 3 (11)	59 ± 6 (58)	31 ± 7 (16)	49 ± 5 (35)	35 ± 18 (8)	45 ± 7 (36)
Junctions (%)						
Symmetrical	43 ± 3 (7)	45 ± 10 (44)	64 ± 8 (30)	64 ± 6 (45)	53 ± 14 (8)	65 ± 4 (50)
Asymmetrical	57 ± 3 (10)	55 ± 10 (51)	36 ± 8 (18)	36 ± 6 (25)	47 ± 14 (9)	35 ± 4 (28)
Symmetrical with dendritic branches	75 ± 14	55 ± 7	74 ± 8	46 ± 13	63 ± 24	55 ± 8
Asymmetrical with dendritic spines	92 ± 8	68 ± 7	38 ± 7	52 ± 17	46 ± 27	54 ± 9

Data from the same varicosities as in Table 1. Means ± SEM from 4 rats with number examined in brackets. The varicosity profiles were classified as showing or not a synaptic junction according to the criteria described in Material and Methods. The synaptic incidence for the whole volume of varicosities was extrapolated from the proportion in single sections by means of the stereological formula of Beaudet and Sotelo (1981), but using the long axis as diameter (Umbriaco et al., 1994). Values greater than 100% suggest the existence of more than one junction per varicosity. *$p < 0.05$ and ***$p < 0.001$ for ACh versus unlabeled. †$p < 0.05$ and ††$p < 0.01$ for PF versus DLG and Rt.

DISCUSSION

This study revealed new aspects of the distribution and fine structural characteristics of the ACh (ChAT-immunostained) innervation in DLG, PF, and Rt of adult rat. Data on the number of ACh axon terminal in each nucleus substantiated the higher density of this innervation in PF and Rt than in DLG. At the electron microscopic level, the data also demonstrated that a majority of ACh axon terminals (varicosities) in Rt and DLG do not establish a synaptic contact, whereas those in PF are significantly larger and entirely synaptic.

Distribution of ACh axon terminals in DLG, PF, and Rt

The experimental conditions of the present study allowed for a specific and optimal immunocytochemical detection of ACh axon varicosities in rat brain tissue (Umbriaco et al., 1994; Mechawar et al., 2000). The ChAT-immunostained axon varicosities were visualized across the full thickness of sections, attesting to a complete penetration of immunoreagents. The immunoreactive varicosities could therefore be counted within the entire thickness of the optical dissector, providing reliable, unbiased estimates of their number per volumetric unit of tissue.

The present counts in DLG, PF, and Rt are in accordance with previous ChAT immunocytochemical investigations of rat thalamus showing a denser ACh innervation in PF and Rt than in DLG (Ichikawa and Hirata, 1986; Levey et al., 1987; Houser et al., 1988). The regional density of innervation was the highest in PF, but Rt, which is traversed by fascicles of myelinated axons, exhibited a higher ratio of ACh axon varicosities per thalamic neuron, because of its lower density in thalamic neurons. DLG was much less densely innervated, in terms both of regional density and of number of ACh terminals per thalamic neuron. However, even in PF and Rt, the regional density of ACh innervation was approximately two-fold lower than in rat neocortex or hippocampus (Mechawar et al., 2000; Aznavour et al., 2005). It should also be pointed out that the density of ACh innervation in DLG has been reported to be considerably higher in the cat (Fitzpatrick et al., 1989), monkey (Wilson et al., 1999), and human (Heckers et al., 1992) than in the rat (Levey et al., 1987), perhaps because of the greater development of the visual system in these species.

Ultrastructural characteristics of ACh axon varicosities

It is obvious from the present and earlier studies (de Lima et al., 1985; Hallanger and Wainer, 1988; Isaacson and Tanaka, 1988; Raczkowski and Fitzpatrick, 1989; Hallanger et al., 1990; Schwartz and Mrzljak, 1993; Patel and Bickford, 1997; Patel et al., 1999) that no morphological features of ACh axon terminals in thalamus would have allowed for their specific electron microscopic identification without immunocytochemical labeling. In the three nuclei examined, these varicosities arose from thin and unmyelinated axons, were generally ovoid, contained aggregated small vesicles, and frequently displayed a mitochondrion. A greater incidence of mitochondria in ACh as opposed to randomly selected, unlabeled varicosity profiles has been previously observed in cat DLG (Raczkowski

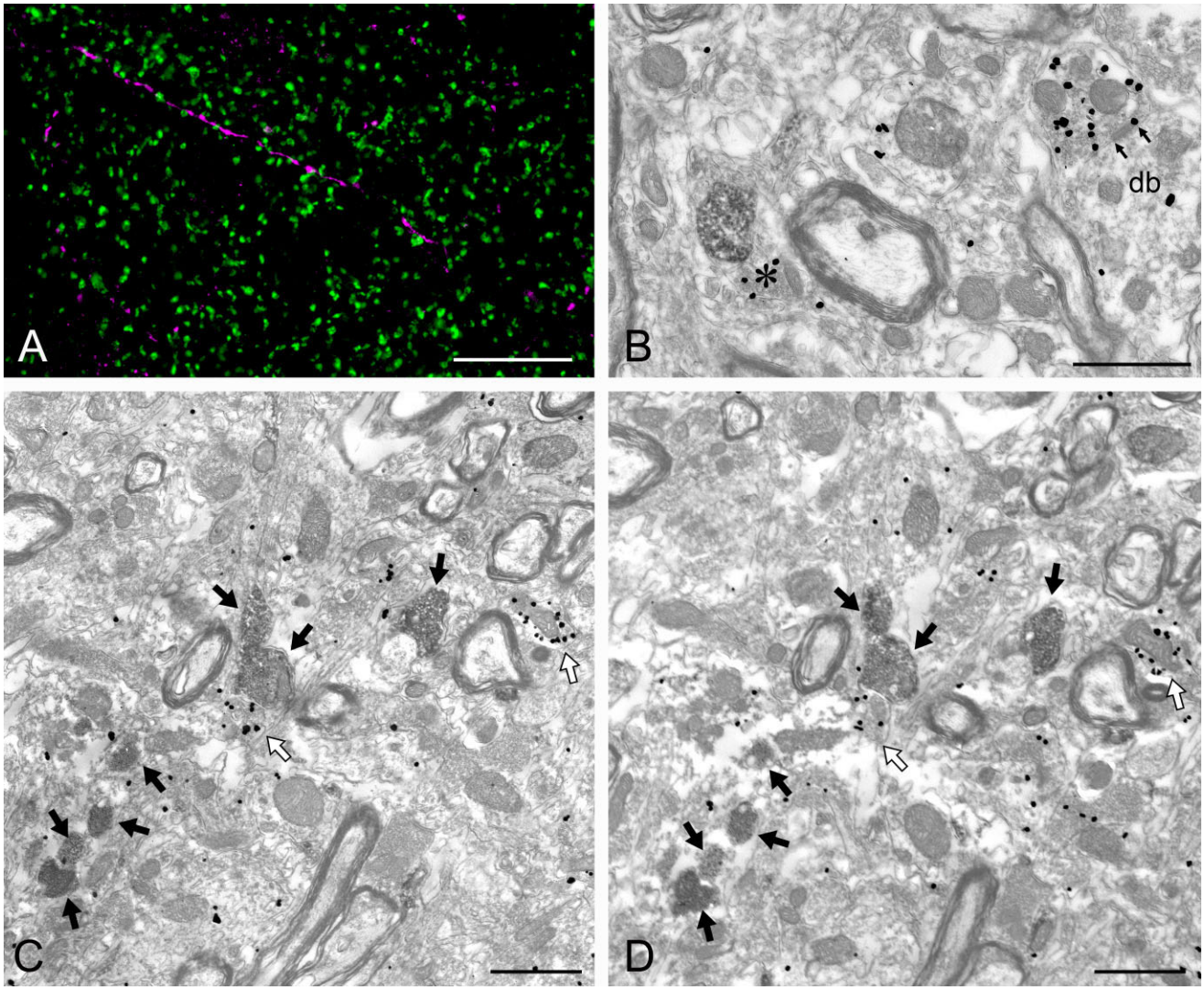

Fig. 5. Confocal (**A**) and electron (**B–D**) microscopic visualization of ChAT- and VGLUT2-immunoreactive axon varicosities in PF, after double immunofluorescence or peroxidase-DAB and immunogold labeling. A: Confocal microscopy. In this merged image, all ChAT axon varicosities (in magenta) aligned on a fiber crossing the field or isolated in the neuropil appear distinct from the numerous VGLUT2 (in green) terminals scattered in the same field. B–D: Examples of DAB-immunolabeled (ChAT) and gold-immunolabeled (VGLUT2) axon varicosities present in the same field. In B, the immunogold-labeled (VGLUT2) varicosity at right exhibits a synaptic junction (between small arrows) on a dendritic branch (db), whereas another one, at lower left (asterisk), lies next to a DAB-labeled (ChAT) varicosity. In C,D, several ChAT-labeled (black arrows) and VGLUT2-labeled (white arrows) axon varicosities are seen in adjacent ultrathin sections across the same field. None of these many axon varicosities are dually labeled. Scale bars = 20 μm in A; 1 μm in B–D.

and Fitzpatrick, 1989) and also in the rat cerebral cortex (Umbriaco et al., 1994; Mechawar et al., 2002), neostriatum (Contant et al., 1996), and hippocampus (Aznavour et al., 2005). Also noteworthy was the larger size of ACh as well as unlabeled axon terminals in PF than in Rt or DLG. In primary somatosensory cortex, larger ACh axon varicosities in layer V, more frequently making synapse than those in other layers, have already been noted (Umbriaco et al., 1994). It was then speculated that anchoring of these varicosities to their microenvironment by junctional complexes might favor the accumulation of inner constituents, which could also be an explanation for the larger size of ACh varicosities in PF compared with Rt and DLG.

The majority of ACh axon terminals in Rt and DLG failed to show the differentiated zones of membrane specialization (junctional complexes) that define synapses. The relatively low synaptic incidence of these varicosities in Rt (39%) and DLG (33%) was all the more striking in that many of the randomly selected unlabeled varicosities in both nuclei, as well as in PF, presumably made more than one synaptic junction. PF was the first example of an entirely synaptic ACh innervation in CNS. Such a difference in synaptic incidence of ACh axon varicosities among thalamic nuclei remains to be explained. There is nothing in the literature to suggest that the ACh innervation of PF and DLG would have distinct neuronal origins. Indeed, there is neuroanatomical evidence indicating that PPN neurons innervate both PF and DLG (Hallanger et al., 1987). Moreover, ACh neurons of the brainstem are presumably endowed with highly collateralized axons (Woolf

and Butcher, 1986; Paré et al., 1988; Steriade et al., 1988; Bolton et al., 1993; Spreafico et al., 1993) likely to innervate both thalamic nuclei. In addition to brainstem neurons, basal forebrain neurons also contribute to the ACh innervation of Rt (Woolf and Butcher, 1986; Hallanger et al., 1987; Levey et al., 1987; Jourdain et al., 1989), but no such projection to PF or DLG has ever been demonstrated in rat.

In the present study, we found no indication that a vesicular glutamate transporter might be present in thalamic ACh axon terminals. Our double-labeling results were consistent with an earlier report of Varoqui et al. (2002), who did not find colocalization of VGLUT2 protein and vesicular acetylcholine transporter (VAChT) in rat brain. This did not exclude a transient expression of a glutamate transporter during development, but refuted the hypothesis that glutamate corelease might be involved in the maintenance of the entirely synaptic ACh innervation in PF.

Functional considerations

It remains to be determined how the observed differences in distribution and ultrastructural features of the ACh innervation among DLG, PF, and Rt might contribute to the diverse functions attributed to these thalamic nuclei. The largely asynaptic character of many innervations in CNS has been viewed as morphological evidence for the existence of diffuse transmission by such neuronal systems, in addition to their synaptic function (reviewed in Descarries and Mechawar, 2008). In the case of ACh, it has also led to the suggestion of the existence of a low, ambient level of neurotransmitter, the fluctuations of which could be implicated in the regulation of a variety of physiological processes mediated by ACh and other transmitter receptors widely distributed on neuronal, glial, and vascular elements (Descarries et al., 1997). Convincing electrophysiological evidence for a regulatory role of ambient ACh has recently been obtained in dual unit recording studies of neostriatum (Narushima et al., 2007; Pakhotin and Bracci, 2007).

Autoradiographic ligand binding studies have demonstrated the existence of abundant nicotinic as well as muscarinic receptor sites in the rat DLG, PF, and Rt (Rotter et al., 1979; Wamsley et al., 1984; Cortes and Palacios, 1986; Mash and Potter, 1986; Spencer et al., 1986; Clarke, 1993). Subsequently, immunocytochemical studies with specific antibodies have provided information on the cellular location of different muscarinic receptor subtypes in the rat DLG and Rt. In DLG, m1 and m3 receptor labeling was found on soma and dendrites of thalamocortical cells, whereas m2 labeling was widespread on soma and dendrites of cells resembling geniculate, GABAergic interneurons (Plummer et al., 1999). In Rt, which is entirely composed of GABAergic neurons, m2 labeling was also abundant (Plummer et al., 1999) and has been described as predominating in distal dendrites and also in the periphery of cell bodies (Oda et al., 2007), where we never found a single synaptic ACh terminal. Thus, in both nuclei, there may be muscarinic receptors postsynaptic to ACh terminals, but a vast majority apparently reside in extrasynaptic locations, where these receptors must be reached by diffusion of ACh. In view of the entirely synaptic ACh innervation of PF, it would be of considerable interest to obtain similar data on muscarinic receptor localization in that nucleus and then compare the effects of ACh in PF to those in DLG and Rt.

According to currently available physiological data, two different mechanisms are postulated to account for the actions of ACh in rat DLG: 1) excitation of thalamocortical neurons and 2) inhibition of DLG interneurons (GABAergic) and of the inhibitory (GABAergic) neurons of Rt that project to other thalamic nuclei, including DLG. To what extent these effects might depend on the synaptic vs. the diffuse mode of transmission by ACh is currently unknown. In vitro physiology suggests that ACh depolarizes thalamocortical cells through effects on both nicotinic and muscarinic receptors, whereas its inhibitory effects on GABAergic geniculate and reticular thalamic neurons would be mediated primarily by muscarinic (m2) receptors. It is assumed that a key role of DLG in vision is to modulate the character of incoming visual signals from retinal ganglion cells en route to primary visual cortex as a function of behavioral state (Singer, 1977; Sherman and Koch, 1986; Steriade and Llinas, 1988; Sherman and Guillery, 1996). The ACh input from the brainstem conveyed to DLG by diffuse as well as synaptic transmission might contribute to this modulation. The maintenance of a low level of ambient ACh in DLG could also play a crucial role in keeping the thalamocortical neurons in the physiological state in which they will respond appropriately to relevant stimuli. Similarly, in Rt, diffuse as well as synaptic ACh transmission could contribute to the maintenance of a majority of its GABAergic neurons in the hyperpolarized state, thus contributing to the disinhibition of thalamocortical neurons located in other thalamic nuclei and to the faithful relay of relevant motor and sensory information to the cerebral cortex during waking.

The intralaminar nuclei, including PF, have been considered as nonspecific thalamic nuclei more involved in the "control of states of consciousness and perceptual awareness" than in the cortical processing of specific information (Jasper, 1960; Van der Werf et al., 2002). This general role is consistent with the finding that PF neurons may innervate large expanses of the cerebral cortex as well as focal areas of neostriatum in the rat and primate (Jones and Leavitt, 1974; Van der Werf et al., 2002; Parent and Parent, 2005). As shown in the present study, PF neurons receive a relatively dense and entirely synaptic ACh input that should allow for the direct relaying of the information from brainstem to both regions. For example, after electrical stimulation of the ipsilateral PPN, half of recorded neurons in rat PF responded by a short latency orthodromic excitation that followed high-frequency stimulation over 300 Hz (Capozzo et al., 2003).

More specific functions have also been assigned to PF, such as attentional orienting to external events, through its thalamostriatal projection (Mancia and Marini, 1995; Minamimoto and Kimura, 2002), and processing of the affective dimension of pain (see, e.g. Harte et al., 2004), presumably through its cortical projections. PF neurons have also been shown to receive afferent projections from output structures of the basal ganglia (van der Kooy and Carter, 1981; Kha et al., 2000; Parent et al., 2001) and have therefore been proposed to provide an important subcortical feedback on striatal output through their thalamostriatal projections (Nauta and Mehler, 1966; Erro et al., 1999; Parent and Parent, 2005). Thus, the direct, synaptic activation of PF neurons by the ACh input from the brainstem during waking must affect basal gan-

glia function, as well as perceptual awareness, including attention and pain perception. PPN has been shown to be reciprocally connected with various basal ganglia components (see Winn, 2006). It is also in a position to affect this set of subcortical structures by exerting a direct ACh control on PF neuronal activity.

ACKNOWLEDGMENTS

The authors are grateful to André Parent for insightful comments on the manuscript.

LITERATURE CITED

Albanese A, Butcher LL. 1980. Acetylcholinesterase and catecholamine distribution in the locus ceruleus of the rat. Brain Res Bull 5:127–134.

Anlauf E, Derouiche A. 2005. Astrocytic exocytosis vesicles and glutamate: a high-resolution immunofluorescence study. Glia 49:96–106.

Aznavour N, Watkins KC, Descarries L. 2005. Postnatal development of the cholinergic innervation in the dorsal hippocampus of rat: quantitative light and electron microscopic immunocytochemical study. J Comp Neurol 486:61–75.

Baxter MG, Chiba AA. 1999. Cognitive functions of the basal forebrain. Curr Opin Neurobiol 9:178–183.

Beaudet A, Sotelo C. 1981. Synaptic remodeling of serotonin axon terminals in rat agranular cerebellum. Brain Res 206:305–329.

Beaulieu C, Cynader M. 1992. Preferential innervation of immunoreactive choline acetyltransferase synapses on relay cells of the cat's lateral geniculate nucleus: a double-labelling study. Neuroscience 47:33–44.

Bolton RF, Cornwall J, Phillipson OT. 1993. Collateral axons of cholinergic pontine neurones projecting to midline, mediodorsal and parafascicular thalamic nuclei in the rat. J Chem Neuroanat 6:101–114.

Capozzo A, Florio T, Cellini R, Moriconi U, Scarnati E. 2003. The pedunculopontine nucleus projection to the parafascicular nucleus of the thalamus: an electrophysiological investigation in the rat. J Neural Transm 110:733–747.

Clarke PB. 1993. Nicotinic receptors in mammalian brain: localization and relation to cholinergic innervation. Prog Brain Res 98:77–83.

Contant C, Umbriaco D, Garcia S, Watkins KC, Descarries L. 1996. Ultrastructural characterization of the acetylcholine innervation in adult rat neostriatum. Neuroscience 71:937–947.

Cortes R, Palacios JM. 1986. Muscarinic cholinergic receptor subtypes in the rat brain. I. Quantitative autoradiographic studies. Brain Res 362:227–238.

Cossette P, Umbriaco D, Zamar N, Hamel E, Descarries L. 1993. Recovery of choline acetyltransferase activity without sprouting of the residual acetylcholine innervation in adult rat cerebral cortex after lesion of the nucleus basalis. Brain Res 630:195–206.

Cozzari C, Howard J, Hartman BK. 1990. Analysis of epitopes on choline acetyltransferase (ChAT) using monoclonal antibobies (Mabs). Program No. 200. Abstract Viewer/Itinerary Planner. Washington, DC: Society for Neuroscience.

de Biasi S, Frassoni C, Spreafico R. 1986. GABA immunoreactivity in the thalamic reticular nucleus of the rat. A light and electron microscopical study. Brain Res 399:143–147.

de Lima AD, Montero VM, Singer W. 1985. The cholinergic innervation of the visual thalamus: an EM immunocytochemical study. Exp Brain Res 59:206–212.

Descarries L, Mechawar N. 2000. Ultrastructural evidence for diffuse transmission by monoamine and acetylcholine neurons of the central nervous system. Prog Brain Res 125:27–47.

Descarries L, Mechawar N. 2008. Structural organization of monoamine and acetylcholine neuron systems in the rat cns. In: Lajtha A, Vizi ES, editors. Handbook of Neurochemistry and Molecular Neurobiology, 3rd ed. New York: Springer. p 1–20.

Descarries L, Gisiger V, Steriade M. 1997. Diffuse transmission by acetylcholine in the CNS. Prog Neurobiol 53:603–625.

Descarries L, Bérubé-Carrière N, Riad M, Bo GD, Mendez JA, Trudeau LE. 2007. Glutamate in dopamine neurons: synaptic versus diffuse transmission. Brain Res Rev 58:290–302.

Deschênes M, Bourassa J, Doan VD, Parent A. 1996. A single-cell study of the axonal projections arising from the posterior intralaminar thalamic nuclei in the rat. Eur J Neurosci 8:329–343.

Donoghue JP, Carroll KL. 1987. Cholinergic modulation of sensory responses in rat primary somatic sensory cortex. Brain Res 408:367–371.

Dykes RW. 1997. Mechanisms controlling neuronal plasticity in somatosensory cortex. Can J Physiol Pharmacol 75:535–545.

Erro E, Lanciego JL, Gimenez-Amaya JM. 1999. Relationships between thalamostriatal neurons and pedunculopontine projections to the thalamus: a neuroanatomical tract-tracing study in the rat. Exp Brain Res 127:162–170.

Fitzpatrick D, Diamond IT, Raczkowski D. 1989. Cholinergic and monoaminergic innervation of the cat's thalamus: comparison of the lateral geniculate nucleus with other principal sensory nuclei. J Comp Neurol 288:647–675.

Fremeau RT Jr, Burman J, Qureshi T, Tran CH, Proctor J, Johnson J, Zhang H, Sulzer D, Copenhagen DR, Storm-Mathisen J, Reimer RJ, Chaudhry FA, Edwards RH. 2002. The identification of vesicular glutamate transporter 3 suggests novel modes of signaling by glutamate. Proc Natl Acad Sci U S A 99:14488–14493.

Fremeau RT Jr, Voglmaier S, Seal RP, Edwards RH. 2004. VGLUTs define subsets of excitatory neurons and suggest novel roles for glutamate. Trends Neurosci 27:98–103.

Gras C, Herzog E, Bellenchi GC, Bernard V, Ravassard P, Pohl M, Gasnier B, Giros B, El Mestikawy S. 2002. A third vesicular glutamate transporter expressed by cholinergic and serotoninergic neurons. J Neurosci 22:5442–5451.

Gras C, Vinatier J, Amilhon B, Guerci A, Christov C, Ravassard P, Giros B, El Mestikawy S. 2005. Developmentally regulated expression of VGLUT3 during early post-natal life. Neuropharmacology 49:901–911.

Graybiel AM, Berson DM. 1980. Autoradiographic evidence for a projection from the pretectal nucleus of the optic tract to the dorsal lateral geniculate complex in the cat. Brain Res 195:1–12.

Graziano A, Liu XB, Murray KD, Jones EG. 2008. Vesicular glutamate transporters define two sets of glutamatergic afferents to the somatosensory thalamus and two thalamocortical projections in the mouse. J Comp Neurol 507:1258–1276.

Hallanger AE, Wainer BH. 1988. Ultrastructure of ChAT-immunoreactive synaptic terminals in the thalamic reticular nucleus of the rat. J Comp Neurol 278:486–497.

Hallanger AE, Levey AI, Lee HJ, Rye DB, Wainer BH. 1987. The origins of cholinergic and other subcortical afferents to the thalamus in the rat. J Comp Neurol 262:105–124.

Hallanger AE, Price SD, Lee HJ, Steininger TL, Wainer BH. 1990. Ultrastructure of cholinergic synaptic terminals in the thalamic anteroventral, ventroposterior, and dorsal lateral geniculate nuclei of the rat. J Comp Neurol 299:482–492.

Harkany T, Hartig W, Berghuis P, Dobszay MB, Zilberter Y, Edwards RH, Mackie K, Ernfors P. 2003. Complementary distribution of type 1 cannabinoid receptors and vesicular glutamate transporter 3 in basal forebrain suggests input-specific retrograde signalling by cholinergic neurons. Eur J Neurosci 18:1979–1992.

Harte SE, Hoot MR, Borszcz GS. 2004. Involvement of the intralaminar parafascicular nucleus in muscarinic-induced antinociception in rats. Brain Res 1019:152–161.

Hasselmo ME. 1995. Neuromodulation and cortical function: modeling the physiological basis of behavior. Behav Brain Res 67:1–27.

Heckers S, Geula C, Mesulam MM. 1992. Cholinergic innervation of the human thalamus: dual origin and differential nuclear distribution. J Comp Neurol 325:68–82.

Herzog E, Bellenchi GC, Gras C, Bernard V, Ravassard P, Bedet C, Gasnier B, Giros B, El Mestikawy S. 2001. The existence of a second vesicular glutamate transporter specifies subpopulations of glutamatergic neurons. J Neurosci 21:RC181.

Herzog E, Gilchrist J, Gras C, Muzerelle A, Ravassard P, Giros B, Gaspar P, El Mestikawy S. 2004. Localization of VGLUT3, the vesicular glutamate transporter type 3, in the rat brain. Neuroscience 123:983–1002.

Hisano S. 2003. Vesicular glutamate transporters in the brain. Anat Sci Int 78:191–204.

Hoover DB, Jacobowitz DM. 1979. Neurochemical and histochemical studies of the effect of a lesion of the nucleus cuneiformis on the cholinergic innervation of discrete areas of the rat brain. Brain Res 170:113–122.

Hoshino K, Katoh YY, Bai W, Kaiya T, Norita M. 2000. Distribution of terminals from pedunculopontine tegmental nucleus and synaptic organization in lateralis medialis-suprageniculate nucleus of cat's thal-

amus: anterograde tracing, immunohistochemical studies, and quantitative analysis. Vis Neurosci 17:893–904.

Houser CR. 1990. Cholinergic synapses in the central nervous system: studies of the immunocytochemical localization of choline acetyltransferase. J Elec Microsc Techn 15:2–19.

Houser CR, Vaughn JE, Barber RP, Roberts E. 1980. GABA neurons are the major cell type of the nucleus reticularis thalami. Brain Res 200: 341–354.

Houser CR, Phelps PE, Vaughn JE. 1988. Cholinergic innervation of the rat thalamus as demonstrated by immunocytochemical localization of choline acetyltransferase. In: Bentivoglio M, Spreafico R, editors. Cellular Thalamic Mechanisms. Amsterdam: Elsevier. p 387–398.

Ichikawa T, Hirata Y. 1986. Organization of choline acetyltransferase-containing structures in the forebrain of the rat. J Neurosci 6:281–292.

Isaacson LG, Tanaka D Jr. 1988. Cholinergic innervation of canine thalamostriatal projection neurons: an ultrastructural study combining choline acetyltransferase immunocytochemistry and WGA-HRP retrograde labeling. J Comp Neurol 277:529–540.

Jacobowitz DM, Palkovits M. 1974. Topographic atlas of catecholamine and acetylcholinesterase-containing neurons in the rat brain. I. Forebrain (telencephalon, diencephalon). J Comp Neurol 157:13–28.

Jasper HH. 1960. Unspecific thalamocortical relations. In: Field J, Magoun HW, Hall VE, editors. Handbook of Physiology. Washington, DC: American Physiological Society. p 1307–1321.

Jasper HH, Tessier J. 1971. Acetylcholine liberation from cerebral cortex during paradoxical (REM) sleep. Science 172:601–602.

Jiménez-Capdeville ME, Dykes RW. 1996. Changes in cortical acetylcholine release in the rat during day and night: differences between motor and sensory areas. Neuroscience 71:567–579.

Jones EG. 2007. The Thalamus. New York: Cambridge University Press.

Jones EG, Leavitt RY. 1974. Retrograde axonal transport and the demonstration of non-specific projections to the cerebral cortex and striatum from thalamic intralaminar nuclei in the rat, cat and monkey. J Comp Neurol 154:349–377.

Jourdain A, Semba K, Fibiger HC. 1989. Basal forebrain and mesopontine tegmental projections to the reticular thalamic nucleus: an axonal collateralization and immunohistochemical study in the rat. Brain Res 505:55–65.

Kaneko T, Fujiyama F, Hioki H. 2002. Immunohistochemical localization of candidates for vesicular glutamate transporters in the rat brain. J Comp Neurol 444:39–62.

Kha HT, Finkelstein DI, Pow DV, Lawrence AJ, Horne MK. 2000. Study of projections from the entopeduncular nucleus to the thalamus of the rat. J Comp Neurol 426:366–377.

Koelle GB. 1954. The histochemical localization of cholinesterases in the central nervous system of the rat. J Comp Neurol 100:211–235.

Kuroda M, Price JL. 1991a. Synaptic organization of projections from basal forebrain structures to the mediodorsal thalamic nucleus of the rat. J Comp Neurol 303:513–533.

Kuroda M, Price JL. 1991b. Ultrastructure and synaptic organization of axon terminals from brainstem structures to the mediodorsal thalamic nucleus of the rat. J Comp Neurol 313:539–552.

Lavoie B, Parent A. 1994. Pedunculopontine nucleus in the squirrel monkey: distribution of cholinergic and monoaminergic neurons in the mesopontine tegmentum with evidence for the presence of glutamate in cholinergic neurons. J Comp Neurol 344:190–209.

Levey AI, Hallanger AE, Wainer BH. 1987. Choline acetyltransferase immunoreactivity in the rat thalamus. J Comp Neurol 257:317–332.

Mancia M, Marini G. 1995. Orienting-like reaction after ibotenic acid injections into the thalamic centre median nucleus in the cat. Arch Ital Biol 134:65–80.

Mash DC, Potter LT. 1986. Autoradiographic localization of M1 and M2 muscarine receptors in the rat brain. Neuroscience 19:551–564.

McCormick DA, Prince DA. 1986. Acetylcholine induces burst firing in thalamic reticular neurones by activating a potassium conductance. Nature 319:402–405.

McKenna TM, Ashe JH, Hui GK, Weinberger NM. 1988. Muscarinic agonists modulate spontaneous and evoked unit discharge in auditory cortex of cat. Synapse 2:54–68.

Mechawar N, Cozzari C, Descarries L. 2000. Cholinergic innervation in adult rat cerebral cortex: a quantitative immunocytochemical description. J Comp Neurol 428:305–318.

Mechawar N, Watkins KC, Descarries L. 2002. Ultrastructural features of the acetylcholine innervation in the developing parietal cortex of rat. J Comp Neurol 443:250–258.

Mesulam MM, Mufson EJ, Wainer BH, Levey AI. 1983. Central cholinergic pathways in the rat: an overview based on an alternative nomenclature (Ch1–Ch6). Neuroscience 10:1185–1201.

Minamimoto T, Kimura M. 2002. Participation of the thalamic CM-Pf complex in attentional orienting. J Neurophysiol 87:3090–3101.

Montana V, Ni Y, Sunjara V, Hua X, Parpura V. 2004. Vesicular glutamate transporter-dependent glutamate release from astrocytes. J Neurosci 24:2633–2642.

Narushima M, Uchigashima M, Fukaya M, Matsui M, Manabe T, Hashimoto K, Watanabe M, Kano M. 2007. Tonic enhancement of endocannabinoid-mediated retrograde suppression of inhibition by cholinergic interneuron activity in the striatum. J Neurosci 27:496–506.

Nauta WJ, Mehler WR. 1966. Projections of the lentiform nucleus in the monkey. Brain Res 1:3–42.

Nauta HJ, Pritz MB, Lasek RJ. 1974. Afferents to the rat caudoputamen studied with horseradish peroxidase. An evaluation of a retrograde neuroanatomical research method. Brain Res 67:219–238.

Ni B, Rosteck PR Jr, Nadi NS, Paul SM. 1994. Cloning and expression of a cDNA encoding a brain-specific Na^+-dependent inorganic phosphate cotransporter. Proc Natl Acad Sci U S A 91:5607–5611.

Ni B, Wu X, Yan GM, Wang J, Paul SM. 1995. Regional expression and cellular localization of the Na^+-dependent inorganic phosphate cotransporter of rat brain. J Neurosci 15:5789–5799.

Nickerson Poulin A, Guerci A, El Mestikawy S, Semba K. 2006. Vesicular glutamate transporter 3 immunoreactivity is present in cholinergic basal forebrain neurons projecting to the basolateral amygdala in rat. J Comp Neurol 498:690–711.

Oda S, Sato F, Okada A, Akahane S, Igarashi H, Yokofujita J, Yang J, Kuroda M. 2007. Immunolocalization of muscarinic receptor subtypes in the reticular thalamic nucleus of rats. Brain Res Bull 74:376–384.

Ohara PT, Lieberman AR, Hunt SP, Wu JY. 1983. Neural elements containing glutamic acid decarboxylase (GAD) in the dorsal lateral geniculate nucleus of the rat; immunohistochemical studies by light and electron microscopy. Neuroscience 8:189–211.

Olivier A, Parent A, Poirier LJ. 1970. Identification of the thalamic nuclei on the basis of their cholinesterase content in the monkey. J Anat 106:37–50.

Ottersen OP, Storm-Mathisen J. 1984. GABA-containing neurons in the thalamus and pretectum of the rodent. An immunocytochemical study. Anat Embryol 170:197–207.

Pakhotin P, Bracci E. 2007. Cholinergic interneurons control the excitatory input to the striatum. J Neurosci 27:391–400.

Paré D, Smith Y, Parent A, Steriade M. 1988. Projections of brainstem core cholinergic and non-cholinergic neurons of cat to intralaminar and reticular thalamic nuclei. Neuroscience 25:69–86.

Parent A, Butcher LL. 1976. Organization and morphologies of acetylcholinesterase-containing neurons in the thalamus and hypothalamus of the rat. J Comp Neurol 170:205–225.

Parent M, Descarries L. 2006. The cholinergic innervation of adult rat thalamus: a quantitative light and electron microscopic immunocytochemical study. Program No. 52.513. Abstract Viewer/Itinerary Planner Washington, DC: Society for Neuroscience Online.

Parent M, Descarries L. 2007. Light and electron microscopic characterization of the acetylcholine innervation in adult rat thalamus. Program No. 67.510. Abstract Viewer/Itinerary Planner Washington, DC: Society for Neuroscience Online.

Parent M, Parent A. 2005. Single-axon tracing and three-dimensional reconstruction of centre median-parafascicular thalamic neurons in primates. J Comp Neurol 481:127–144.

Parent M, Lévesque M, Parent A. 2001. Two types of projection neurons in the internal pallidum of primates: single-axon tracing and three-dimensional reconstruction. J Comp Neurol 439:162–175.

Patel NC, Bickford ME. 1997. Synaptic targets of cholinergic terminals in the pulvinar nucleus of the cat. J Comp Neurol 387:266–278.

Patel NC, Carden WB, Bickford ME. 1999. Synaptic targets of cholinergic terminals in the cat lateral posterior nucleus. J Comp Neurol 410:31–41.

Paxinos G, Watson C. 2005. The Rat Brain in Stereotaxic Coordinates. Burlington, VT: Academic Press.

Plummer KL, Manning KA, Levey AI, Rees HD, Uhlrich DJ. 1999. Muscarinic receptor subtypes in the lateral geniculate nucleus: a light and electron microscopic analysis. J Comp Neurol 404:408–425.

Raczkowski D, Fitzpatrick D. 1989. Organization of cholinergic synapses in the cat's dorsal lateral geniculate and perigeniculate nuclei. J Comp Neurol 288:676–690.

Rasmusson DD, Dykes RW. 1988. Long-term enhancement of evoked potentials in cat somatosensory cortex produced by coactivation of the basal forebrain and cutaneous receptors. Exp Brain Res 70:276–286.

Riad M, Garcia S, Watkins KC, Jodoin N, Doucet E, Langlois X, el Mestikawy S, Hamon M, Descarries L. 2000. Somatodendritic localization of 5-HT1A and preterminal axonal localization of 5-HT1B serotonin receptors in adult rat brain. J Comp Neurol 417:181–194.

Richter D, Crossland J. 1949. Variation in acetylcholine content of the brain with physiological state. Am J Physiol 159:247–255.

Rotter A, Birdsall NJ, Burgen AS, Field PM, Hulme EC, Raisman G. 1979. Muscarinic receptors in the central nervous system of the rat. I. Technique for autoradiographic localization of the binding of [^{3}H]propylbenzilylcholine mustard and its distribution in the forebrain. Brain Res 180:141–165.

Sarter M, Bruno JP, Givens B. 2003. Attentional functions of cortical cholinergic inputs: what does it mean for learning and memory? Neurobiol Learn Mem 80:245–256.

Sarter M, Hasselmo ME, Bruno JP, Givens B. 2005. Unraveling the attentional functions of cortical cholinergic inputs: interactions between signal-driven and cognitive modulation of signal detection. Brain Res Brain Res Rev 48:98–111.

Schafer MK, Varoqui H, Defamie N, Weihe E, Erickson JD. 2002. Molecular cloning and functional identification of mouse vesicular glutamate transporter 3 and its expression in subsets of novel excitatory neurons. J Biol Chem 277:50734–50748.

Scheibel ME, Scheibel AB. 1966. The organization of the nucleus reticularis thalami: a Golgi study. Brain Res 1:43–62.

Schwartz ML, Mrzljak L. 1993. Cholinergic innervation of the mediodorsal thalamic nucleus in the monkey: ultrastructural evidence supportive of functional diversity. J Comp Neurol 327:48–62.

Sherman SM, Guillery RW. 1996. Functional organization of thalamocortical relays. J Neurophysiol 76:1367–1395.

Sherman SM, Koch C. 1986. The control of retinogeniculate transmission in the mammalian lateral geniculate nucleus. Exp Brain Res 63:1–20.

Shute CC, Lewis PR. 1963. Cholinesterase-containing systems of the brain of the rat. Nature 199:1160–1164.

Shute CC, Lewis PR. 1967. The ascending cholinergic reticular system: neocortical, olfactory and subcortical projections. Brain 90:497–520.

Sillito AM, Kemp JA. 1983. Cholinergic modulation of the functional organization of the cat visual cortex. Brain Res 289:143–155.

Singer W. 1977. Control of thalamic transmission by corticofugal and ascending reticular pathways in the visual system. Physiol Rev 57: 386–420.

Sofroniew MV, Priestley JV, Consolazione A, Eckenstein F, Cuello AC. 1985. Cholinergic projections from the midbrain and pons to the thalamus in the rat, identified by combined retrograde tracing and choline acetyltransferase immunohistochemistry. Brain Res 329:213–223.

Somogyi J, Baude A, Omori Y, Shimizu H, El Mestikawy S, Fukaya M, Shigemoto R, Watanabe M, Somogyi P. 2004. GABAergic basket cells expressing cholecystokinin contain vesicular glutamate transporter type 3 (VGLUT3) in their synaptic terminals in hippocampus and isocortex of the rat. Eur J Neurosci 19:552–569.

Spencer DG Jr, Horvath E, Traber J. 1986. Direct autoradiographic determination of M1 and M2 muscarinic acetylcholine receptor distribution in the rat brain: relation to cholinergic nuclei and projections. Brain Res 380:59–68.

Spreafico R, Amadeo A, Angoscini P, Panzica F, Battaglia G. 1993. Branching projections from mesopontine nuclei to the nucleus reticularis and related thalamic nuclei: a double labelling study in the rat. J Comp Neurol 336:481–492.

Steriade M. 2004. Acetylcholine systems and rhythmic activities during the waking-sleep cycle. Prog Brain Res 145:179–196.

Steriade M, Llinas RR. 1988. The functional states of the thalamus and the associated neuronal interplay. Physiol Rev 68:649–742.

Steriade M, McCarley RW. 2005. Brain Control of Sleep and Wakefulness. New York: Academic Press.

Steriade M, Paré D, Parent A, Smith Y. 1988. Projections of cholinergic and non-cholinergic neurons of the brainstem core to relay and associational thalamic nuclei in the cat and macaque monkey. Neuroscience 25:47–67.

Steriade M, Dossi RC, Paré D, Oakson G. 1991. Fast oscillations (20–40 Hz) in thalamocortical systems and their potentiation by mesopontine cholinergic nuclei in the cat. Proc Natl Acad Sci U S A 88:4396–4400.

Stichel CC, Singer W. 1985. Organization and morphological characteristics of choline acetyltransferase-containing fibers in the visual thalamus and striate cortex of the cat. Neurosci Lett 53:155–160.

Takamori S, Rhee JS, Rosenmund C, Jahn R. 2001. Identification of differentiation-associated brain-specific phosphate transporter as a second vesicular glutamate transporter (VGLUT2). J Neurosci 21: RC182.

Trudeau LE. 2004. Glutamate cotransmission as an emerging concept in monoamine neuron function. J Psychiatry Neurosci 29:296–310.

Umbriaco D, Watkins KC, Descarries L, Cozzari C, Hartman BK. 1994. Ultrastructural and morphometric features of the acetylcholine innervation in adult rat parietal cortex: an electron microscopic study in serial sections. J Comp Neurol 348:351–373.

van der Kooy D, Carter DA. 1981. The organization of the efferent projections and striatal afferents of the entopeduncular nucleus and adjacent areas in the rat. Brain Res 211:15–36.

Van der Werf YD, Witter MP, Groenewegen HJ. 2002. The intralaminar and midline nuclei of the thalamus. Anatomical and functional evidence for participation in processes of arousal and awareness. Brain Res Brain Res Rev 39:107–140.

Varoqui H, Schafer MK, Zhu H, Weihe E, Erickson JD. 2002. Identification of the differentiation-associated Na^+/PI transporter as a novel vesicular glutamate transporter expressed in a distinct set of glutamatergic synapses. J Neurosci 22:142–155.

Vincent SR, Kimura H. 1992. Histochemical mapping of nitric oxide synthase in the rat brain. Neuroscience 46:755–784.

Vincent SR, Reiner PB. 1987. The immunohistochemical localization of choline acetyltransferase in the cat brain. Brain Res Bull 18:371–415.

Vincent SR, Satoh K, Fibiger HC. 1986. The localization of central cholinergic neurons. Prog Neuropsychopharmacol Biol Psychiatry 10:637–656.

Wamsley JK, Gehlert DR, Roeske WR, Yamamura HI. 1984. Muscarinic antagonist binding site heterogeneity as evidenced by autoradiography after direct labeling with [^{3}H]-QNB and [^{3}H]-pirenzepine. Life Sci 34:1395–1402.

Wilson JR, Manning KA, Forestner DM, Counts SE, Uhlrich DJ. 1999. Comparison of cholinergic and histaminergic axons in the lateral geniculate complex of the macaque monkey. Anat Rec 255:295–305.

Winn P. 2006. How best to consider the structure and function of the pedunculopontine tegmental nucleus: evidence from animal studies. J Neurol Sci 248:234–250.

Wong-Riley M. 1979. Changes in the visual system of monocularly sutured or enucleated cats demonstrable with cytochrome oxidase histochemistry. Brain Res 171:11–28.

Woolf NJ, Butcher LL. 1986. Cholinergic systems in the rat brain: III. Projections from the pontomesencephalic tegmentum to the thalamus, tectum, basal ganglia, and basal forebrain. Brain Res Bull 16:603–637.

Zhou J, Nannapaneni N, Shore S. 2007. Vessicular glutamate transporters 1 and 2 are differentially associated with auditory nerve and spinal trigeminal inputs to the cochlear nucleus. J Comp Neurol 500:777–787.